Optica Applicata, Vol. XLIII, No. 3, 2013
DOI: 10.5277/oa130310

Phase features of several typical blood cells and their identification without unwrapping

YAWEI WANG[1], YUJIAO CHEN[1*], CUIHONG LÜ[1], XUEFU SHANG[1], YUANYUAN XU[1], HUI WU[1], XINGLONG ZHU[2], WEIFENG JIN[2]

[1]Faculty of Science, Jiangsu University, Zhenjiang, Jiangsu 212013, China

[2]School of Mechanical Engineering, Jiangsu University, Zhenjiang, Jiangsu 212013, China

[*]Corresponding author: chenyujiao993@163.com

The digital holographic phase microscopy (DHPM) technique which has been proposed for cellular morphology and dynamic analysis yielded highly desirable results. However, for nucleated cells (especially white blood cells (WBCs)), their submicroscopic structure has not yet been deconstructed through a phase unwrapping method due to the heterogeneity of an internal phase. By analyzing the phase heterogeneity of subclasses of WBCs, the typical phase models of them are built first in this paper; using the simulation method, the wrapped phase distributions of these models are obtained. However, by optimizing the wrapped phase maps and analyzing the relationships between them and typical blood cells, their features are selected and extracted. Then the models built are sorted out from each other successfully without unwrapping via analyzing these extracted features, which provides a valuable approach and technological base for the classification and identification of blood cells.

Keywords: digital holographic phase, nucleated cell, phase model, wrapped phase features, identification.

1. Introduction

Classification and counting of human blood cells are of great significance for diagnosis and treatment of blood diseases. The phase distribution is closely bound up with the structural form due to the transparent property of blood cell, so it can be used as an important basis for sorting cells [1]. In recent years, digital holographic phase microscopy (DHPM) has been proposed for biological cell detection [2–5], which develops rapidly and has several advantages such as high precision, high speed, real-time online and full field of view. The representative applications of DHPM are as follows: Fourier phase microscopy (FPM) [6, 7], Hilbert phase microscopy (HPM) [8–10], diffraction phase microscopy (DPM) [11, 12], *etc*. Recently, white light diffraction phase microscopy (wDPM) and direct phase imaging method without transformation also have been proposed [13, 14]. According to the wide applications of DHPM, it can be seen that the analysis and deconstruction of phase information have developed and achieved good results. However, all these methods can be only applied to the detection

of homogeneous phase structures like the red blood cell (RBC). There is no suitable phase unwrapping method which could be used for the observation and measurement of heterogeneous cells due to their complicated internal structures.

Therefore, in the present paper, the optical features of typical blood cells are analyzed, especially those of white blood cells (WBCs), and based on the results, the phase models of RBCs and subgroups of WBCs are built. Using simulation technology, the wrapped phase distributions corresponding to these models are obtained. Then several features of these phase maps are selected and extracted through analyzing the relationships between them and the structure of cells. By assembling and optimizing these features, the models are sorted successfully without unwrapping, which can overcome the drawbacks of the identification method of heterogeneous cell phase, and offers a valuable basis for the science and technology of cell detection.

2. Models of typical blood cells

RBCs and WBCs are important components of blood, and mature WBCs can be separated into five subcategories as follows: lymphocyte, monocyte, neutrophil, eosinophil and basophil. The shapes of blood cells are various, which is closely related to the growth state and disease. In general, RBCs are shaped like a disc – the diameter is 7–8 μm, the center is biconcave and the thickness is about 1 μm, at the edge the thickness is about 2 μm, and the normal RBC is a nucleate when mature. For the five subgroups of WBCs, they are generally shaped like a ball or an ellipsoid, the differences among them are the diameter and nucleus. Neutrophil is 10–15 μm in diameter with the nucleus being bacilliform or lobulated; lymphocyte is 6–15 μm in diameter with the nucleus being spherical or ellipsoidal; monocyte is 12–20 μm in diameter with the nucleus being kidney-shaped or U-shaped; eosinophil is 13–15 μm in diameter with the nucleus being mostly bi-lobed or glasses-shaped; basophil is 10–12 μm in diameter with the nucleus being lobulated or S-shaped.

We have yielded some achievements in studying the modeling of blood cells [15, 16], and according to the structure parameters mentioned above, the typical models of RBCs and WBCs are built in this paper. The morphological parameters of each model are listed below: the RBC model is a biconcave disc, the central thickness is 1 μm, the thickness at the edge is 2 μm, and the diameter is 7.7 μm; all WBC models are 12 μm-diameter spheres with nucleuses of different shapes. The morphological structure of typical blood cells and their corresponding three-dimensional models are shown in Fig. 1.

3. Phase imaging by simulation

Based on the plane wave interference principle and according to the actual parameters of optical path of the digital phase microscopy, the simulation of the above cell models are performed through an optical virtual simulation platform of VirtualLab whose reliability has been demonstrated [1, 17].

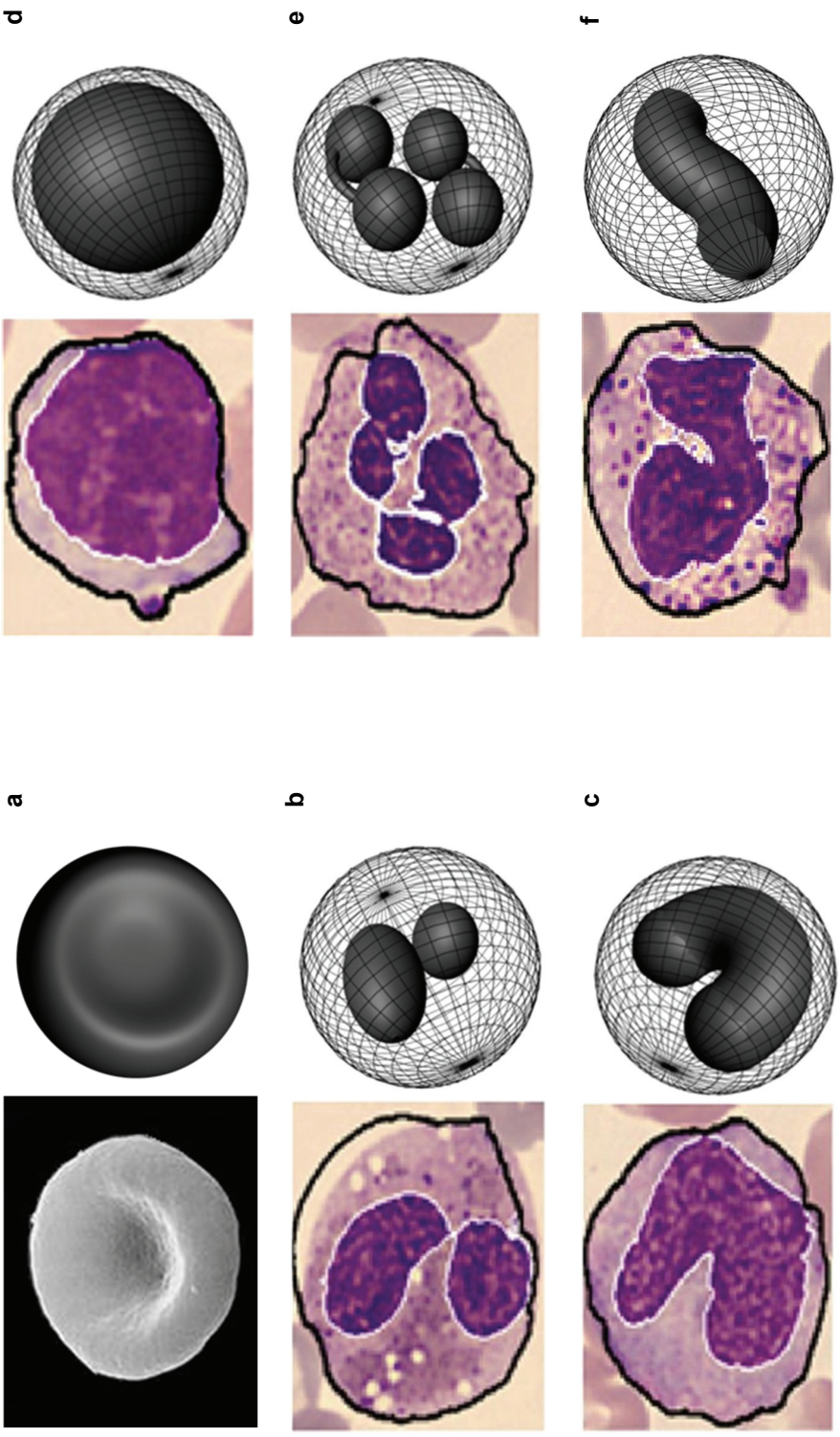

Fig. 1. Morphological structure of typical blood cells and their corresponding three-dimensional models: RBC (**a**), lymphocyte (**b**), eosinophil (**c**), neutrophil (**d**), monocyte (**e**), basophil (**f**).

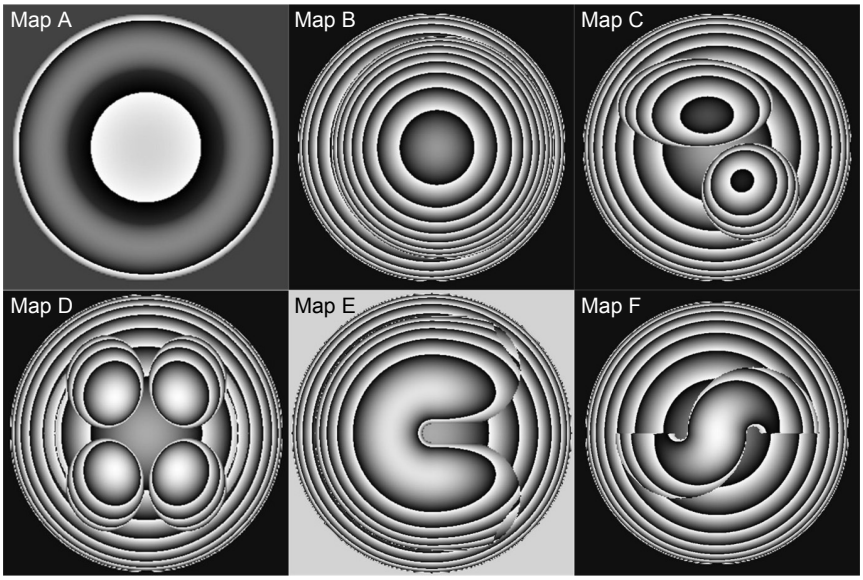

Fig. 2. The wrapped phase maps A–F corresponding to the models in Figs. 1**a**–1**f**, respectively.

The experiment parameters are set as follows. The light source is a plane wave; the input field shape is a 40 μm-diameter circle; the wavelength is 532 nm; the spectral weight is 1; the relative edge width is 3%; the lateral offset is 0; the refractive index of extracellular medium is 1.0003; the sampling distance is 50 nm×50 nm; the size of embedding frame is 10; the type of polarization is linearly polarized; the direction of incidence is normal incidence; the propagation operator is *thin element approximation*. The refractive index and absorption coefficient of cytoplasm of all models are 1.3375 and 0.1/m, respectively; the refractive index and absorption coefficient of nucleuses are 1.5866 and 0.130531/m, respectively. The phase maps obtained are shown in Fig. 2.

4. Feature analysis and extraction

4.1. Texture feature

From Figure 2, we can find that there are obvious differences among textures of each wrapped phase map. According to the theory of interference phase imaging, the relationship between the phase distribution Φ and the refractive index as well as the thickness can be expressed as [18]

$$\Phi = \frac{2\pi\left[(n_1 - n_0)h_1 + (n_2 - n_1)h_2\right]}{\lambda} \tag{1}$$

where n_0 is the refractive index of the extracellular medium, n_1 is the refractive index of cytoplasm, n_2 is the refractive index of nucleus, and $n_1 < n_2$, λ is the wavelength of

light source, h_1 and h_2 are thickness of cell and nucleus, respectively. If n_c is used for representing the average refractive index of the whole cell, the formula (1) can be approximately simplified as:

$$\Phi = \frac{2\pi(n_c - n_0)h_1}{\lambda} \tag{2}$$

For RBC, $n_c = n_1$, the density of equal phase is sparse near the center because the center is biconcave. For WBCs, because $n_1 < n_2$, $n_1 < n_c < n_2$, the density of equal phase increases. So the phase distribution is closely related to nucleus, and it is important to note that the shape and number of nucleus also have a great effect on a phase map pattern.

Texture is generally formed by the spatial distribution of gray level, so there is a gray correlation property on space between two pixels in an image. Gray-level co-occurrence matrix (GLCM) is a classic second-order statistical method, which is often used to analyze and classify the texture image, and achieves good results. GLCM reflects the comprehensive information of gray level on direction, spacing and the range of variation, which is defined as a tabulation of how often different combinations of pixel gray levels occur in an image. The mathematical expression is

$$P(i, j, \delta, \theta) = \left\{ \left[(x, y), (x + \Delta x, y + \Delta y) \right] \middle| f(x, y) = i,\ f(x + \Delta x, y + \Delta y) = j; \right.$$
$$\left. x = 0, 1, \ldots, N_{x-1};\ y = 0, 1, \ldots, N_{y-1} \right\} \tag{3}$$

where $i, j = 0, 1, 2, \ldots, L - 1$, L is the gray level, $\delta = (\Delta x^2 + \Delta y^2)^{1/2}$, θ is the direction of generating GLCM, x, y are coordinates of pixel, N_x, N_y are the number of rows and columns, respectively.

Various statistics can be extracted from GLCM for describing texture, and in this paper, entropy, contrast and energy are selected as features. Entropy reflects the randomness of texture, the value of it is greatest when all values of GLCM are equal, lower when the values of GLCM are very uneven. It can be described by

$$\mathrm{ENT} = -\sum_i \sum_j P(i - j) \log \left[P(i, j) \right] \tag{4}$$

Contrast is the moment of inertia near the principal diagonal of GLCM, which is used for measuring the distribution of matrix value and the local changes in an image. It reflects the definition of image and the depth of texture grooves, which can be expressed as

$$\mathrm{CON} = \sum_i \sum_j (i - j)^2 P(i, j) \tag{5}$$

T a b l e 1. Texture features.

Map	ENT	CON	ASM	Q
A	3.4993	0.1121	0.6830	0.5743
B	6.3416	1.4575	0.1683	54.9191
C	6.4650	0.9379	0.1713	35.3971
D	6.5345	1.0920	0.1812	39.3801
E	6.0407	1.0646	0.2292	28.0582
F	6.0677	0.9211	0.2303	24.3682

Energy is the sum of the squares of all GLCM elements, which is also named second-order moment. It reflects the even degree of gray distribution and the coarseness of texture, and the equation is

$$\mathrm{ASM} = \sum_i \sum_j P(i, j)^2 \tag{6}$$

And finally, we define that

$$Q = \frac{\mathrm{ENT} \times \mathrm{CON}}{\mathrm{ASM}} \tag{7}$$

Each map in Fig. 2 is calculated, and the results are shown in Table 1.

By comparing the Q value in Table 1, it can be found that there is a great difference between map A and others, so texture can be taken as a feature.

4.2. Nucleus feature

Through the analysis in Section 4.1, we know that the shape and number of nuclei have a great effect on a phase map pattern. In order to analyze the nucleus in isolation, each map in Fig. 2 is segmented, except Fig. 2**a**. After binarization, denoising, expansion

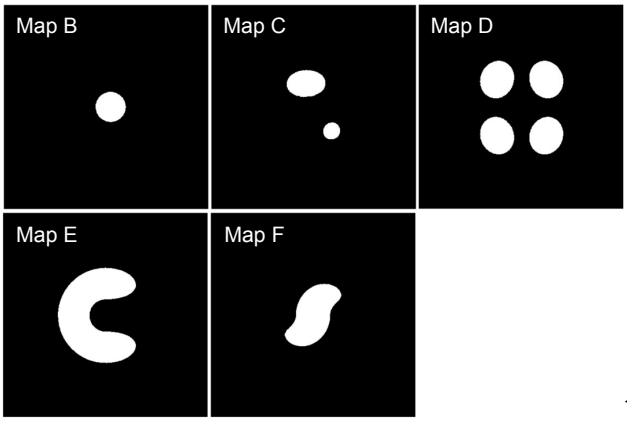

◀ Fig 3. The segmented maps.

T a b l e 2. The number *N* of extracted domains

Map	B	C	D	E	F
N	1	2	4	1	1

and corrosion, the connected domain without a hole is extracted and counted. The segmented maps are shown in Fig. 3 and *N* is used as the symbol for the number of extracted domains which is shown in Table 2.

4.2.1. The number of nuclei

Combining Figure 3, Table 2 and the corresponding cell models, it can be easily found that *N* is equal to the number of nuclei whose shape can be reflected by the extracted domains approximately. So *N* can be taken as a feature, maps C and D can be sorted out from Table 2.

4.2.2. The shape of nucleus

Rotundity degree – ε is chosen as the symbol for a rotundity degree, which is defined as

$$\varepsilon = \frac{4\pi S}{L^2} \tag{8}$$

where S is the area, L is the perimeter. When the geometric is close to round, ε is close to 1. The rotundity degree of Fig. 3 (maps B, E and F) is calculated and the results are shown in Table 3.

T a b l e 3. Rotundity degree ε of extracted domains.

Map	B	E	F
ε	0.9107	0.4349	0.6950

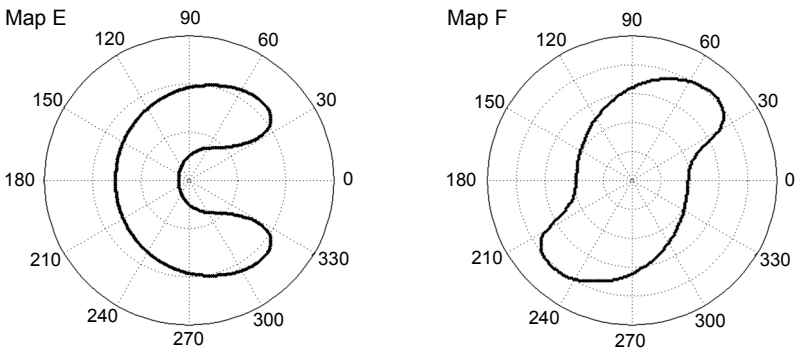

Fig. 4. The fringe contour in a polar coordinate system.

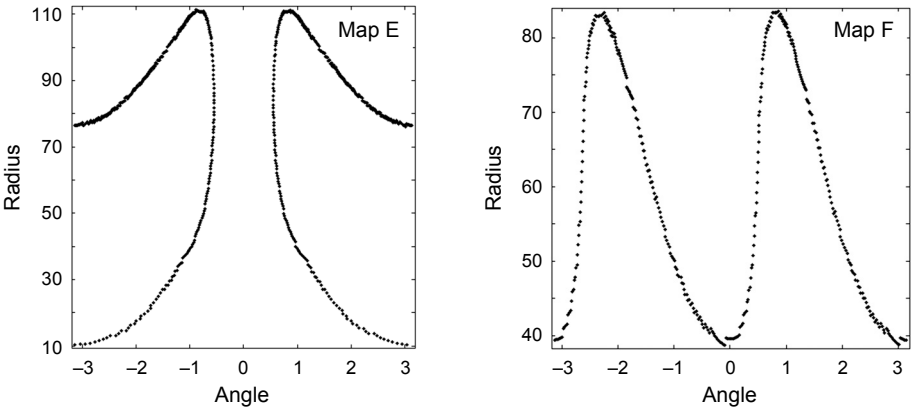

Fig. 5. The fringe contour painted with the angle as *X*-axis and radius as *Y*-axis.

Comparing Tab. 3 with Fig. 3, we can find that the ε value of map B is the maximum and closest to 1 because the nucleus is spherical.

The relative position of peaks – We extracted the fringe of Fig. 3 (maps E and F), and took the centroid of an extracted domain as the pole, then transformed the coordinate from the Cartesian coordinate system to the polar coordinate system: the derived fringe maps are shown in Fig. 4. Then, the fringe contour of Fig. 4 is painted with the angle as *X*-axis and radius as *Y*-axis as shown in Fig. 5.

From Figure 5, we can see that there are two peaks in each map. For map E, the two peaks are located in the adjacent quadrants because the nucleus is U-shaped; for map F, the two peaks are located in the opposite quadrants because the nucleus is S-shaped. So the relative position of peaks can be selected as a feature.

5. Conclusions

Although there are some differences in morphology between the cell phase model built in this paper and the real cell, the structure morphology of nucleated cell is well expressed. The simulation of those typical blood cell models are executed using virtual simulation technology and the corresponding wrapped phase maps are obtained. The analysis of these maps suggests that the distribution features of a wrapped phase are closely related to the number and morphology of a nucleus, thus the texture feature and nucleus feature are extracted, and the models are sorted out from each other successfully. Based on the above analysis and discussion, a texture feature can be used for sorting RBCs out from WBCs and the method advanced in the present paper can extract nucleus feature effectively, which can be used as the reference for classifying WBCs. The thresholds of classification are determined by the actual situation in practical applications. This method also can be applied to classify other biological

nucleated cells. The present paper provides a valuable method and technical basis for classification and identification of heterogeneous cells.

Acknowledgements – This work was supported by the National Natural Science Foundation of China (No. 11374130), the PhD Programs Foundation of the Ministry of Education of China (No. 20113227-110018), Colleges and Universities Major Project of Jiangsu Province (No. 09KJA140001) and Nantong of Jiangsu Project AS2011015.

Reference

[1] WANG Y.W., HAN G.C., LIU Y., CHENG X.N., WYROWSKI F., *Simulation study on phase distribution of blood cells by virtual imitation*, Chinese Journal of Lasers **36**, 2009, pp. 1595–1600.

[2] KEMPER B., KOSMEIER S., LANGEHANENBERG P., VON BALLY G., BREDEBUSCH I., DOMSCHKE W., SCHNEKENBURGER J., *Integral refractive index determination of living suspension cells by multi-focus digital holographic phase contrast microscopy*, Journal of Biomedical Optics **12**(5), 2007, article 054009.

[3] RAPPAZ B., CANO E., COLOMB T., KÜHN J., DEPEURSINGE C., SIMANIS V., MAGISTRETTI P.J., MARQUET P., *Noninvasive characterization of the fission yeast cell cycle by monitoring dry mass with digital holographic microscopy*, Journal of Biomedical Optics **14**(3), 2009, article 034049.

[4] KHMALADZE A., MATZ R.L., EPSTEIN T., JASENSKY J., BANASZAK HOLL M.M., ZHAN CHEN, *Cell volume changes during apoptosis monitored in real time using digital holographic microscopy*, Journal of Structural Biology **178**(3), 2012, pp. 270–278.

[5] XIAOXU LU, JIANPEI CHEN, SHENGDE LIU, ZHIJIAN MA, ZHUN ZHANG, LIYUN ZHONG, *3D profile reconstruction of biological sample by in-line image-plane phase-shifting digital microscopic holography*, Optics and Lasers in Engineering **50**(10), 2012, pp. 1431–1435.

[6] POPESCU G., DEFLORES L.P., VAUGHAN J.C., BADIZADEGAN K., IWAI H., DASARI R.R., FELD M.S., *Fourier phase microscopy for investigation of biological structures and dynamics*, Optics Letters **29**(21), 2004, pp. 2503–2505.

[7] POPESCU G., BADIZADEGAN K., DASARI R.R., FELD M.S., *Observation of dynamic subdomains in red blood cells*, Journal of Biomedical Optics **11**(4), 2006, article 040503.

[8] POPESCU G., IKEDA T., BEST C.A., BADIZADEGAN K., DASARI R.R., FELD M.S., *Erythrocyte structure and dynamics quantified by Hilbert phase microscopy*, Journal of Biomedical Optics **10**(6), 2005, article 060503.

[9] LUE N., BEWERSDORF J., LESSARD M.D., BADIZADEGAN K., DASARI R.R., FELD M.S., POPESCU G., *Tissue refractometry using Hilbert phase microscopy*, Optics Letters **32**(24), 2007, pp. 3522–3524.

[10] LUE N., CHOI W., POPESCU G., YAQOOB Z., BADIZADEGAN K., DASARI R.R., FELD M.S., *Live cell refractometry using Hilbert phase microscopy and confocal reflectance microscopy*, Journal of Physical Chemistry A **113**(47), 2009, pp. 13327–13330.

[11] POPESCU G., IKEDA T., DASARI R.R., FELD M.S., *Diffraction phase microscopy for quantifying cell structure and dynamics*, Optics Letters **31**(6), 2006, pp. 775–777.

[12] YONGKEUN PARK, BEST C.A., BADIZADEGAN K., DASARI R.R., FELD M.S., KURIABOVA T., HENLE M.L., LEVINE A.J., POPESCU G., *Measurement of red blood cell mechanics during morphological changes*, Proceedings of the National Academy of Sciences of the United States of America **107**(15), 2010, pp. 6731–6736.

[13] BHADURI B., PHAM H., MIR M., POPESCU G., *Diffraction phase microscopy with white light*, Optics Letters **37**(6), 2012, pp. 1094–1096.

[14] RU WANG, ZHUO WANG, MILLET L., GILLETTE M.U., LEVINE A.J., POPESCU G., *Dispersion-relation phase spectroscopy of intracellular transport*, Optics Express **19**(21), 2011, pp. 20571–20579.

[15] WANG Y.W., HAN G.C., LIU Y., CHENG X.N., WYROWSKI F., *Light scattering virtual simulation of red blood cell under double curve symmetrical model*, Chinese Journal of Lasers **34**, 2007, pp. 1676–1681.

[16] XU Y.Y., WANG Y.W., JIN W.F., JIANG S.W., YUE Q.W., BU M., SHANG X.F., LV C.H., *Study on phase characteristics of white blood cells and their optical models*, Chinese Journal of Lasers **39**, 2012, article 0504001.

[17] WANG Y.W., LEI H.N., BU M., HAN G.C., *Distribution characteristics and identification of several typical blood cells under optical phase models*, Chinese Journal of Lasers **36**, 2009, pp. 2629–2635.

[18] YAWEI WANG, WEIFENG JIN, NAIFEI REN, *Dual-medium quantitative measurement simulation on cells*, Applied Optics **50**(35), 2011, pp. 6440–6445.

Received November 3, 2012